Aerodynamic Interaction in a Three Rotor Tandem Configuration

Jaime J. González Pérez
jaigonp2@etsid.upv.es

Instituto Superior Técnico, Universidade de Lisboa, Portugal

October 2022

Abstract

The aim of this work is to evaluate the impact of several parameters (rotor diameter, interaxial and interplanar separations and rotation speed) on the performance of partially overlapping tandem rotor configurations. It is pretended to contribute to the development of alternative drone configurations with the attained results, in particular to tandem configurations present in drones with two rotor planes. An outline of Momentum Theory is presented as a first-approximation analysis of isolated rotors, along with an existing adaptation of the theory for tandem-rotor configurations accounting for the rotor interaction. A modification of this model is proposed so that it also takes in regard the interplanar separation other than the interaxial distance. A testing bench originally developed for the study of coaxial configurations for two small rotors has been adapted for the study of tandem configurations of up to three rotors. The instruments are capable of measuring the thrust and torque produced by them, and the calibration of the setup was verified with performance data provided by the manufacturer and with CFD simulations data. Several CFD simulations were carried out with CAD models which highly resemble the original propellers. The rotor interaction was successfully captured in regard to thrust loss. The downstream rotor performance was found to be very sensitive to the interaxial separation and to the upstream rotor angular velocity, while the upstream rotor diameter variation had an intermediate impact and the effect of the interplanar separation was slight.
Keywords: Drone, Tandem-rotor Configuration, Experimental Analysis, CFD, Aerodynamic Interaction

1. Introduction

The use of drones or unmanned aerial vehicles (UAVs) is becoming increasingly popular in a lot of areas of application. Aerial imaging, surveillance, weather forecasting or the delivery of goods are just some of the fields which benefit from the use of drones, due to either profitability, effectiveness or safety over human labor. However, the quadrotor performance is awfully vulnerable to the malfunction of a motor, losing the capability to balance the moments in all of the three axes simultaneously. Since drones are progressively becoming a part of everyday life, the safety issue raises concern specially when civilian areas are involved. Moreover, for applications in which heavier loads are to be transported, the thrust produced by only four rotors is limited if the overall UAV dimensions and the noise emissions are contemplated.

The answer to both of the latter complications is the addition of extra rotors. Hexarotor or octorotor configurations are not only able to provide for more thrust without necessarily increasing the rotor size and arm length or the rotation speed, but also they can bear with a rotor fail while maintaining the controllability of the system by rearranging the power distribution on the rest of motors. Alternative configurations with two rotor planes (which allow for larger propellers mounted) separated by a vertical distance have been explored by some researchers, such as Zhu et al. [1], who carried out a study on the performance of several octorotor configurations with rotors divided in two rotor planes.

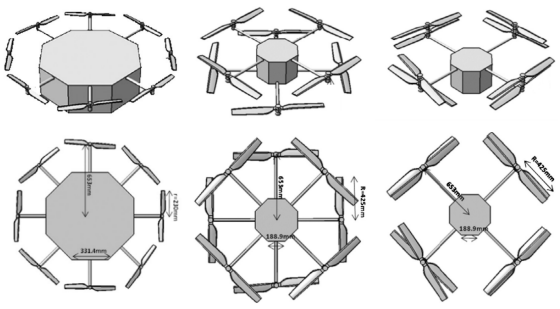

Figure 1: Single rotor plane, tandem-like and pure coaxial configurations [1]

It is pointed out that when a rotor plane is rotated 45° with respect to the other, the resulting tandem-like configuration yields a better performance than that of pure coaxial rotors, while allowing for grater rotor diameters without having to extend the drone arms, as shown in Fig. 1.

However, tandem configurations have their drawbacks: an aerodynamic interaction will appear between rotors, which will specially affect the downstream rotors under a wake, reducing the developed thrust of the overall system and increasing the power needed. It is important to study this phenomenon and find design lines that make the most out of tandem configurations. In order to do that, throughout this work the effect of several relevant parameters on the tandem configuration performance (mainly on the back rotors thrust) such as rotor diameters, rotor speed and interplanar and interaxial distances and will be assessed through experimental and computational fluid dynamics (CFD) approaches.

2. Theoretical Background

The Momentum Theory Analysis (MTA) is broadly used as a first-order approximation in isolated rotor analyses [2]. The relevant performance parameters for isolated rotors as well as theory modifications for tandem rotor configurations are presented.

The required power to hover depends on the thrust T, the rotor area A and the air density ρ, as Eq. 1 shows:

$$P_{\text{ideal}} = \frac{T^{3/2}}{\sqrt{2\rho A}} \tag{1}$$

The Figure of Merit FM is a hover efficiency parameter, defined as the ratio of the ideal power needed to hover and the actual power used, the mechanical power (Eq. 2):

$$FM = \frac{P_{\text{ideal}}}{P_{\text{mech}}} \tag{2}$$

2.1. Momentum Theory for Tandem Rotors

Two approaches for tandem rotors of equal diameter and assumed to produce the same thrust (upstream rotor thrust equal to downstream rotor thrust, $T_u = T_d$) are presented by Leishman [2] using the MTA. The first is applicable for rotors in close proximity (interplanar distance $h \approx 0$), while the second approach is adequate if the downstream rotor is under the fully developed wake of the upstream rotor ($h \to \infty$), where the upstream rotor is assumed to remain undisturbed by the downstream rotor. The latter approach has been modified in this work to allow for intermediate h separations.

These models are based on the assumption that the power required to hover is proportional to the ratio of area overlapped to the total rotor area, $m' = A_{\text{ov}}/A$, which increases as the interaxial separation between rotors d decreases. In tandem rotors, the overlap coefficient κ_{ov} is defined as the ratio of induced power required to hover with overlap (with tandem interaction) to the total induced power required by two isolated rotors, as Eq. 3 shows. κ_{ov} is evaluated for the ratio of interaxial distance to the downstream rotor diameter d/D_{d} (which produces a certain overlap ratio m') for the two cases stated previously.

$$\kappa_{\text{ov}} = \frac{P_{\text{ind}_{\text{ov}}}}{P_{\text{ind}}} \tag{3}$$

1. For $h \approx 0$ the rotors are in close proximity, and the resulting expression for κ_{ov} is:

$$\kappa_{\text{ov}} = 1 + \left(\sqrt{2} - 1\right) m' \tag{4}$$

2. For $h \to \infty$, the downstream rotor is under the fully developed wake of the upstream rotor. However, this approach has been adapted for any h between no vertical separation ($h = 0$) and fully developed wake separation ($h \to \infty$, although a certain fully developed wake distance h_{dw} needs to be established), still maintaining the assumption that the upstream rotor is not affected by the downstream rotor. The overlap is now considered to be produced between the downstream rotor area and the upstream rotor wake area, which shrinks as it develops vertically although its velocity increases due to the mass conservation hypothesis on the closed wake stream tube. The wake stream tube boundaries (and consequently the wake area with the h separation) are modelled with hyperbolic tangent functions and the flow velocity along the stream tube is modelled according to the mass conservation. The resulting κ_{ov} is:

$$\kappa_{\text{ov}} = \frac{\left(G\left(m', \chi\right) + 1 + \chi m'\right)}{2} \tag{5}$$

Where χ is a coefficient representing the flow velocity (non-linearly a function of h, and ranging from 1 to 2, for $h = 0$ and $h = h_{\text{dw}}$ respectively), and $G\left(m', \chi\right)$ is a non-linear function of χ and m' (which now is also a function of h besides of d since the wake shrinks as h increases). Note that the original Leishman [2] approach can be obtained by setting $\chi = 2$ and $h = h_{\text{dw}}$.

The comparison of the two approaches for tandem rotor configurations are presented in Fig. 2. A d/D_{d} ratio of 0 means complete overlap between upstream and downstream rotors, whereas a ratio of 1 equals to no overlap between rotors. The solid lines represent the original Leishman [2] approaches, while the dashed lines belong to the modified approach accounting for the several h distances ranging from 0 to h_{dw}. The left plateau found on the rotor in wake approach appears because the wake area is totally overlapped with the back rotor area, and maintains a constant value until a certain d distance is reached, whereas the right plateau appears when the wake area is no longer overlapped with the back rotor area.

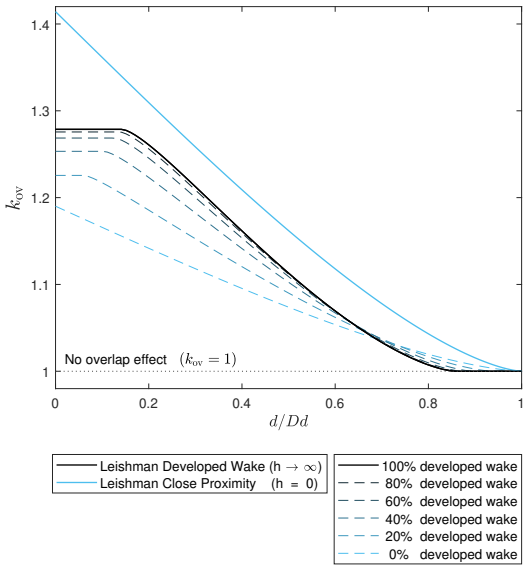

Figure 2: Graphical comparison of κ_{ov}. Solid lines for the Leishman theoretical approaches and dashed lines for the modified Leishman approach (accounting for intermediate vertical distances)

3. Experimental Approach and Methodology

The thrust and torque on the instrumented tube (IT) mounted propellers (particularly those of the back rotor on IT1) are the desired data, so that in the tandem configuration the values can be compared to those of the isolated propellers, assessing the effect of the aerodynamic interaction.

3.1. Experimental Test Bench

The experimental set-up is an adaptation from the original test bench designed by Amado [3], which allowed for the study of coaxial configuration (capable of rotor-plane separation, referred to as h distance). The original test bench had two ITs on top of which two brushless direct current (BLDC) electric motors where placed along the propellers to test. IT1 had 3 strain gage bridges allowing it to measure the forces (F_x and F_y) and the torque (M_x) produced by the propeller, while IT2 only measures torque. Additionally, they were provided angular velocity Ω sensors located above the BLDC motors, and current and voltage sensors connected to the motors. The setup was later modified by Santos [4] to allow for tandem configuration (introduction of interaxial distance d) and in this work a third (uninstrumented) tube (UT) was added in the back rotor plane for flow symmetry, using the same power width modulation (PWM) signal as the other back rotor mounted on IT1 (Figs. 3 and 4).

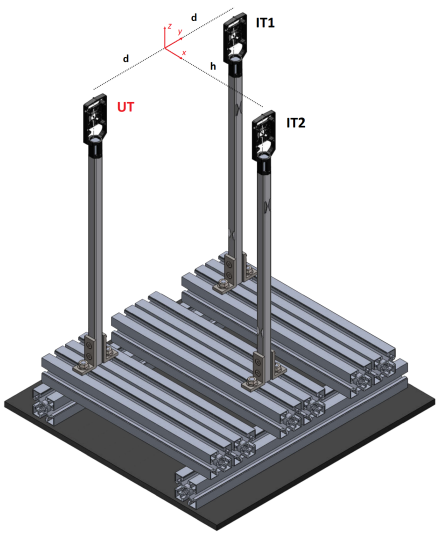

Figure 3: Test bench sketch along with the frame of reference and the h and d separations

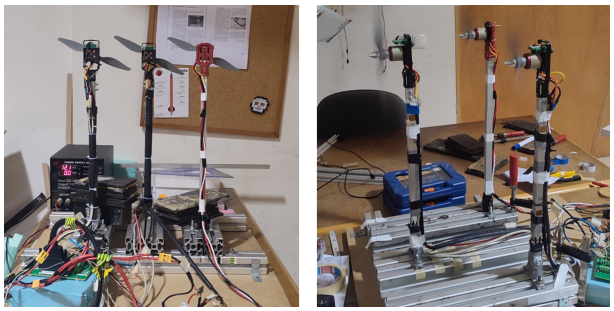

Figure 4: Pictures of the final test bench

The data acquisition and the control of the system are both handled by the Labview [5] software. The inputs to the test bench are the PWM signals for the motors, and the outputs are the current and voltage measures on the IT motors, the strain gages measures and the RPM of the IT motors. The RPM measurements are feedbacked into Labview for the proportional control loops of the front and back rotors planes PWM signals. A block diagram of this configuration is presented in Fig. 5.

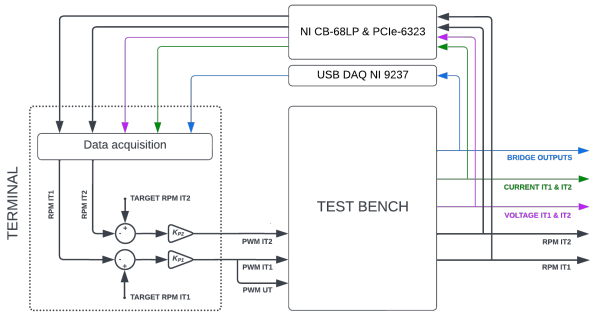

Figure 5: Block diagram of the inputs, outputs and control loops of the system

3.2. Test Bench Verification

The verification of the test bench calibration and measurements is carried out by the comparison of the experimentally obtained thrust and torque values for several APC [6] propellers at different rotation speeds, the 10×6E, 9×6E and 8×6E (in $D \times P$ format, where D is the rotor diameter in inches and P is the propeller pitch in inches/revolution), with the values provided by the propeller manufacturer APC [7] and those obtained with CFD simulations (Figs. 6 and 7).

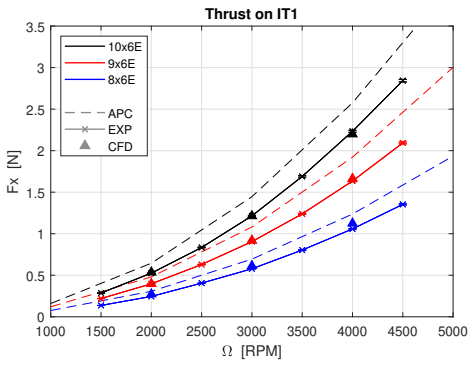

Figure 6: APC, CFD and computed experimental values of thrust (F_x) for the isolated propellers

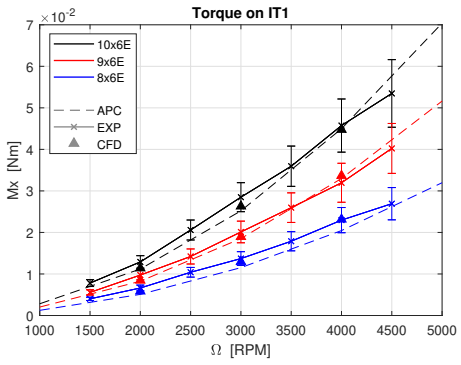

Figure 7: APC, CFD and computed experimental values of torque (M_x) for the isolated propellers

The APC values have been obtained with the NASA Transonic Airfoil Analysis Computer Program [8], which uses the vortex theory on several blade profiles along the propeller span. APC warns that the thrust and torque may not match experimental results in all scenarios, as it can be seen in Figs. 6 and 7 (thrust is overpredicted, up to a 15.95% higher on average for APC 10×6E, and torque is slightly underpredicted for low speeds), although the experimental and CFD results are very similar.

3.3. Test Plan

The experimental tests are carried out with a three rotor tandem configuration in hover condition (no incoming flow), with propellers of equal pitch, with the same direction of rotation and with the two back rotors using the same propeller and rotating at the same speed. The parameters of study are:

- **Interplanar distance** h. Three separations are studied, [90, 150, 210] mm.
- **Interaxial distance** d. Four separations are studied, [140, 160, 180, 210] mm.
- **Front and back rotors speed Ω_F and Ω_B.** Three speeds ([2000, 3000, 4000] RPM) were tested on each rotor plane, resulting in 9 possible combinations of front and back rotors speed.
- **Front and back rotor diameters**. The combinations of propellers are:

Table 1: Propeller diameter combinations tested experimentally

Front Rotor	Back Rotors
10×6E	10×6E 9×6E 8×6E
9×6E	9×6E 8×6E
8×6E	8×6E

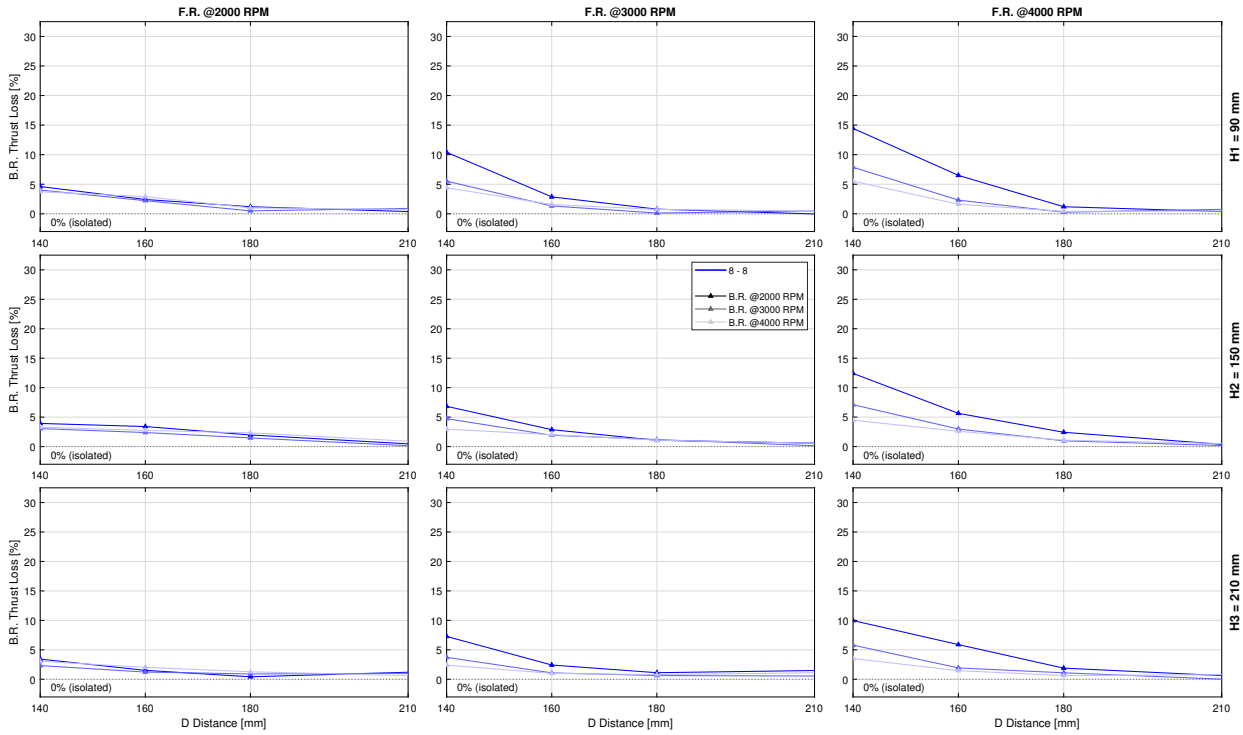

Figure 8: Percentage thrust loss with respect to the isolated rotor values, for all d, h and rotor speeds combinations for propeller configurations with APC 8×6E as front rotor

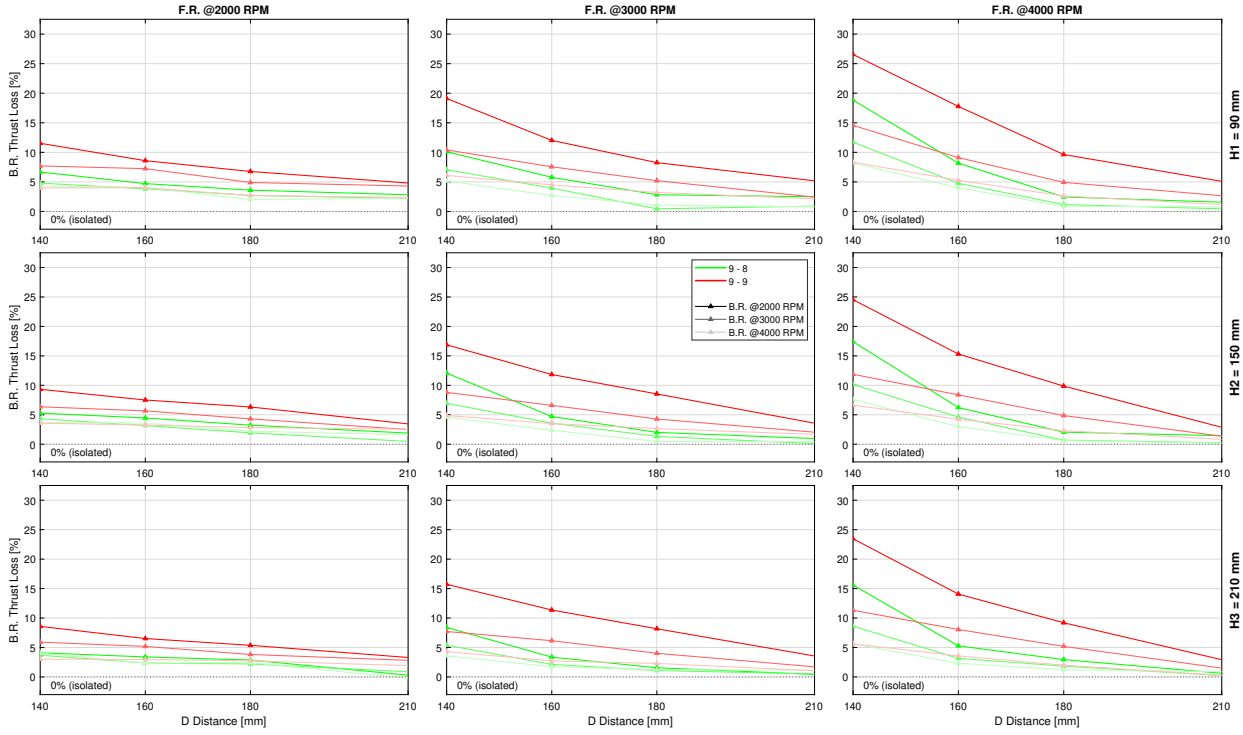

Figure 9: Percentage thrust loss with respect to the isolated rotor values, for all d, h and rotor speeds combinations for propeller configurations with APC 9×6E as front rotor

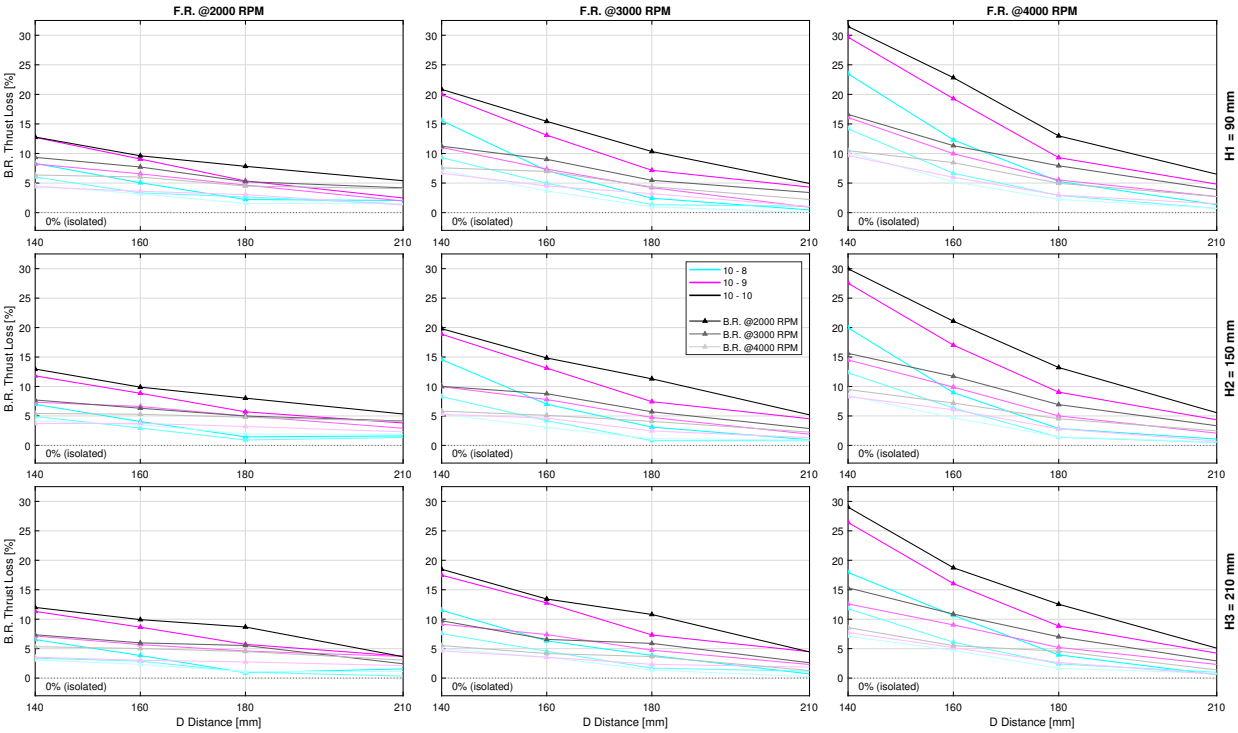

Figure 10: Percentage thrust loss with respect to the isolated rotor values, for all d, h and rotor speeds combinations for propeller configurations with APC 10×6E as front rotor

4. Computational Fluid Dyanimcs Appoach and Methodology

Some of the tests carried out experimentally are performed with computational fluid dynamics (CFD) simulations using the STAR-CCM+ software [9] with own 3D computer aided design (CAD) models built from the geometric data of the propellers provided by the manufacturer APC [6].

4.1. 3D Modelling of the Propellers

APC provides data sheets of their propellers where the several airfoils along the span are described with geometric data such as the chord, the profiles used, the pitch, the thickness ratio etc. A script was developed in Matlab [10] so that this information was transformed into several airfoil 3D coordinates to be exported into Solidworks [11], for any APC propeller in their electric family (example in Figs. 11 and 12).

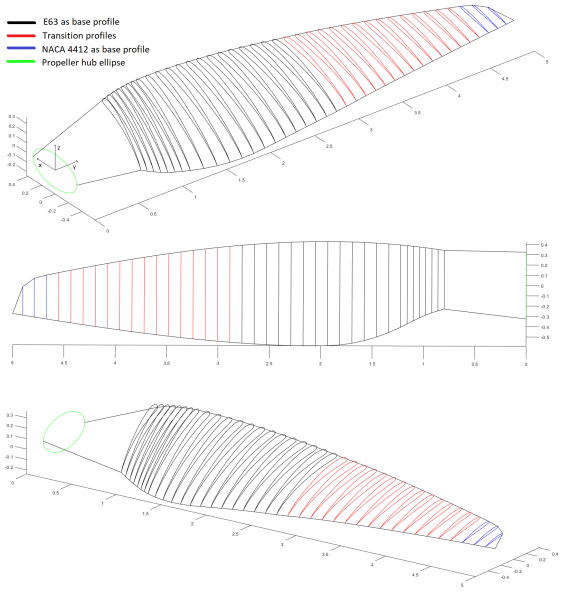

Figure 11: Airfoil sections, leading edge and trailing edge lines for the APC 10×5.5MR

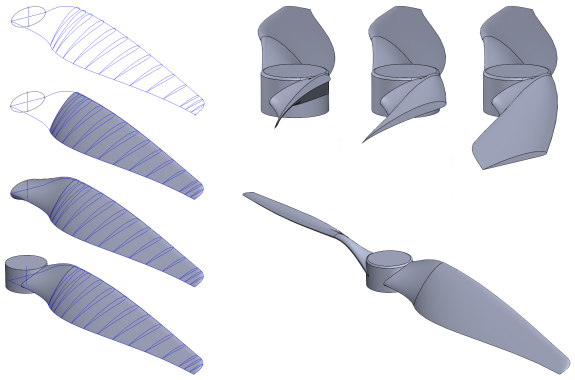

Figure 12: APC 10×6E CAD procedure and result

4.2. CFD simulation methodology

Due to the unsteady nature of the study case, the approach chosen to model the rotating motion is the Rotating Mesh method [12], in which there is a static mesh and a rotating mesh connected by an interface, and the position of the latter updates every time step. The CFD simulations are carried out on the isolated propeller 10×6E with the properties on Tab. 2:

Table 2: Simulation and mesh properties

Approach	Rotating Mesh
Δ_t discretization scheme	Implicit 1st order
Δ_x discretization scheme	Upwind 2nd order
Solver	Segregated
Turbulence model	SST $k-\omega$
Rotating mesh	Polyhedral
Static mesh	Hexahedral

For the 10×6E, the best solutions balanced with computational cost which also grant a solution independent of the mesh (maximum variation of a 1%) in thrust and torque values are found for time steps equivalent to 5° of rotation, 30 sub-iterations, 1.1×10^6 cells on the rotating mesh and 7 prism layers with a stretching of 1.5 (total thickness 0.83 mm). The values of thrust and torque are averaged for 5 propeller turns after the transient, and the resulting values for all the isolated propellers are shown in Figs. 6 and 7 (very similar to the experimental results). A visualisation of the mesh properties applied on the tandem configuration is shown in Fig. 13, although due to computational cost, the simulations are carried out with only two propellers (Fig. 14) (30% time saved and negligible difference on the back rotor performance).

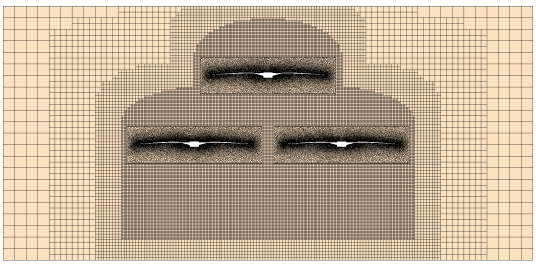

Figure 13: Mesh cut with three 10×6E propellers

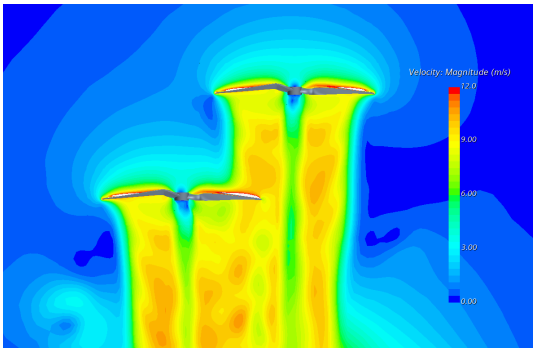

Figure 14: Wake interaction velocity plot

5. Results

The test bench torque measures were very affected by the IT position changes (wire movement, manual attachment and detachment of the screws etc.), which made it impossible to find any trend with the h and d separations for torque, so only the thrust loss on the back rotor with reference to the isolated values is presented. Regarding the CFD approach, also only the thrust is presented since the simulations are not able to capture the effect of the upstream wake on the downstream propeller. Presumably much finer meshes and smaller time steps are required to correctly evaluate the wake nature and the skin forces (torque), although the pressure forces (thrust) yield good results.

5.1. Experimental Results

The percentage thrust loss on the back rotor with respect to the isolated case is presented for all of the 648 tests in Figs. 8, 9 and 10. The impact of the study variables are:

- The thrust loss increases as the distance d decreases. Its impact is very high, since the portion of back rotor area affected by the front rotor wake increases (turbulent wake that disturbs the flow on the propeller and may cause separation).
- The thrust loss increases as the h distance decreases, since the front rotor wake shrinks as it develops in the streamwise direction. The

effect is slight and more noticeable for small d distances.

- The percentage thrust loss increases as the front rotor speed Ω_F increases (wake more turbulent and energetic), and it decreases as Ω_B increases since the back rotor produces more thrust and its baseline flow is more difficult to disturb. Both parameters are very important.

- All of the previous effects were empowered by the rotor diameter combination, since as the d separations are fixed, the diameters determine the percentage area overlap between rotors. Larger rotors (either in front or back rotor planes) result in larger thrust loss on the back rotor due to the increased overlap (and wake disturbance). Besides, an additional cause for large front rotors to cause greater thrust losses is the increased tip speed for the same rotation speed (leading to more turbulent and disturbing wakes).

- The thrust loss is represented against the percentage area overlap on the back rotor for all the tests in Fig. 15. It can be noticed that with increasing overlap (produced by larger rotors or smaller d separations), the thrust loss increases. Besides, the dispersion between the greatest and smallest thrust losses for every equal overlap column (for $\Omega_F = 4000$ RPM, $\Omega_B = 2000$ RPM, $h = 90$ mm and $d = 140$ mm leading to the greatest thrust loss, and $\Omega_F = 2000$ RPM, $\Omega_B = 4000$ RPM, $h = 210$ mm and $d = 210$ mm for the smallest) grows with the overlap. The dispersion is minimum for small and maximum for large back rotor propellers (combinations involving 8×6E and 10×6E as back rotors).

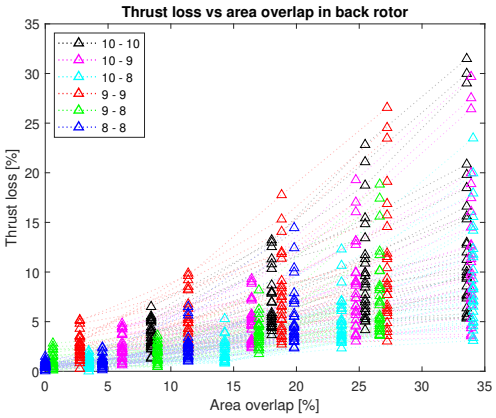

Figure 15: Back rotor thrust loss versus percentage area overlap

5.2. CFD Results

Some of the experimental tests were performed with CFD with two rotors to evaluate the thrust loss on the back rotor and compare with experimental results through two sensitivity studies. The first study involved the d and h separations variation with constant front and back rotors speeds of 4000 RPM, using two APC 9×6E propellers. The second study involved the variation of the back rotor speed with a constant front rotor speed of 4000 RPM for the fixed separations $h = 90$ mm and $d = 140$ mm (for two propeller combinations, 9×6E - 9×6E and 10×6E - 9×6E).

The h and d separations study results are presented in Fig. 16. Despite the simulations being carried with 2 rotors instead of 3 and the rest of sources of error, the tendency in thrust loss is followed quite accurately, with the maximum differences in percentage thrust loss appearing for the smallest d separations where there is more overlap.

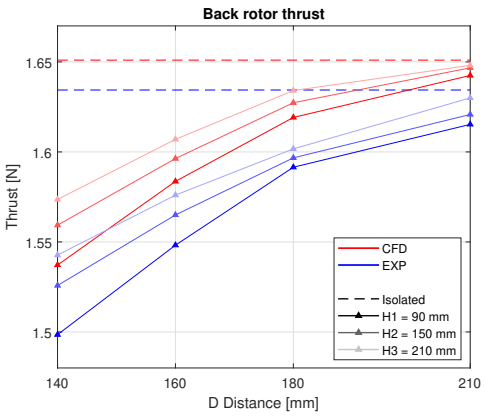

(a) Back rotor thrust

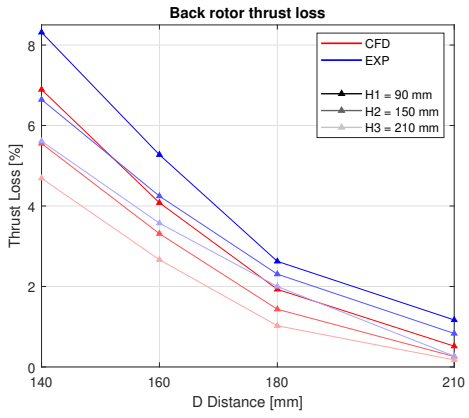

(b) Back rotor thrust loss

Figure 16: Back rotor thrust and back rotor thrust loss for the h and d sensitivity study

As for the back rotor speed sensitivity study, the thrust on the back rotor for the double 9×6E pro-

peller combination is presented in Fig. 17.

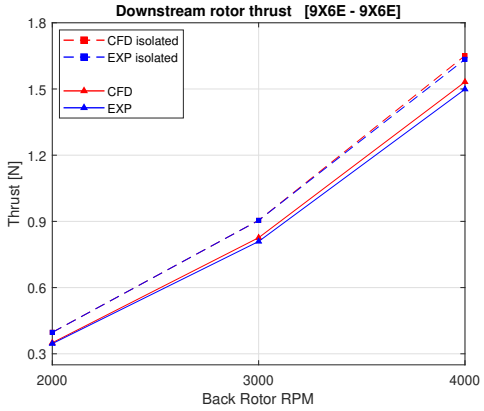

Figure 17: Back rotor thrust for the back rotor speed sensitivity study (9×6E as front rotor)

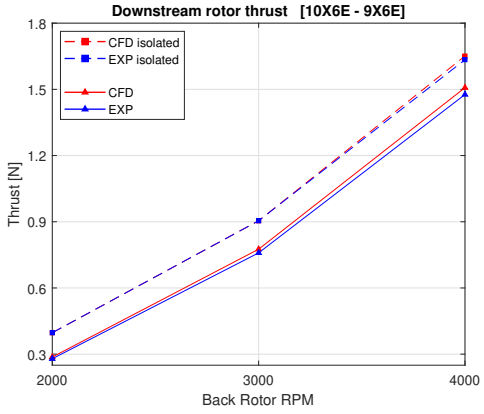

Figure 18: Back rotor thrust for the back rotor speed sensitivity study (10×6E as front rotor)

It can be noticed that the CFD values follow quite precisely the thrust trends obtained experimentally (higher thrust loss with respect to the isolated values for lower back rotor speeds, and even higher losses for a larger front rotor), although the CFD values are always slightly greater than those obtained experimentally (due to all of the sources of error introduced by the experimental setup, the degree of precision of the simulations, a single back rotor instead of two, the absence of the tubes modelled in the simulations etc.). In the back rotor speed sensitivity study, the maximum percentage thrust loss differences between the experimental and the CFD values are all below a 2%.

6. Conclusions

The present study provides a quantitative insight of some of the parameters that affect the performance of tandem rotor configurations with small sized propellers, as those which would be implemented on UAVs with two rotor planes.

The interaxial distance d proved to have a great impact on the back rotor thrust loss with respect to the isolated rotor values, along with the rotation speeds of the rotors Ω_F and Ω_B, and the rotor diameters. The effect of the interplanar separation h was slight in comparison to those previously mentioned. Regarding the CFD simulations, the obtained results for thrust loss on the back rotor follow the experimentally obtained trends, although to properly evaluate the effect that the upstream rotor wake has on torque computationally, a much higher computational cost is presumably required (for isolated rotors with no wake interaction it was enough with the simulation parameters chosen along the study to obtain thrust and torque values very similar to the experimental ones).

6.1. Future Work

The experimental setup could be improved, or at least new ways of changing the position of the ITs should be found so that the process is less invasive and acceptable variations of torque with the h and d distances can be obtained, entailing the evaluation of relevant parameters in rotorcrafts that require the mechanical power P_{mech}, such as the FM (which has only been evaluated for the isolated rotors) or κ_{ov}. Regarding the CFD simulations, if a computational cluster was available, the mesh and simulations parameters required for obtaining good torque values with tandem configurations could be explored, and the simulations could run faster and even include the third rotor due to the increased computational power available. In general, other parameters that seem relevant could be added to the study, such as the propeller pitch, the effect different directions of rotation, the number of blades per propeller or the flight condition (only hover is analysed, but others such as axial climb or forward flight could be applied by introducing the test bench into the available wind tunnel).

Acknowledgements

I must thank my supervisors Filipe Cunha and José Raul Azinheira for granting me the opportunity to work on this project and for their advice, concern and help throughout it. I must also thank professors José Manuel Pereira and Pedro Martí for their advice in the computational fluid dynamics field, my laboratory mate Carlos Vasconcelos for his cooperation during these months and Henrique Santos for his help in the test bench matters. I do not forget about my family and friends, specially my mother, Jaime, Schahde, Josep and Teresa, whose support made this easier. Thank you all.

References

[1] He Zhu, Hong Nie, Limao Zhang, Xiao Hui Wei, and M. Zhang. Design and assessment of octocopter drones with improved aerodynamic efficiency and performance. *Aerospace Science and Technology*, 106:106206, 2020.

[2] J. Gordon Leishman. *Principles of helicopter aerodynamics*, volume 12 of *Cambridge aerospace series*. Cambridge University Press, 2nd edition, 2006. ISBN:0521660602.

[3] Inês Silva Amado. Experimental comparison of planar and coaxial rotor configurations in multi-rotors. 2017. MSc Thesis, Instituto Superior Técnico, Lisboa.

[4] Henrique Antunes Portela Santos. Aerodynamic interactions between tandem configuration rotors. 2021. MSc Thesis, Instituto Superior Técnico, Lisboa.

[5] National Instruments. Labview webpage, 2022. Available online at: https://www.ni.com/pt-pt/shop/labview.html, last accessed on 15.09.2022.

[6] APC propellers. APC propellers webpage, 2022. Available online at: https://www.apcprop.com/, last accessed on 15.09.2022.

[7] APC propellers. APC propellers performance data, 2022. Available online at: https://www.apcprop.com/technical-information/performance-data/, last accessed on 15.09.2022.

[8] F. Carroll Dougherty, Terry L. Holst, Kaitlyn Grundy, and Scott D. Thomas. Tair: A transonic airfoil analysis computer code. 1994.

[9] Siemens. Simcenter STAR-CCM+ webpage, 2022. Available online at: https://www.plm.automation.siemens.com/global/en/products/simcenter/STAR-CCM.html, last accessed on 15.09.2022.

[10] Mathworks. Matlab webpage, 2022. Available online at: https://es.mathworks.com/products/matlab.html, last accessed on 15.09.2022.

[11] Dassault Systems. Solidworks webpage, 2022. Available online at: https://www.solidworks.com/, last accessed on 15.09.2022.

[12] Runa Pinto, Asif Afzal, Loyan D'Souza, Zahid Ansari, and Mohammad Samee. Computational fluid dynamics in turbomachinery: A review of state of the art. *Archives of Computational Methods in Engineering*, 24, 2016.